ARL-TR-7825 ● SEP 2016

US Army Research Laboratory

A Novel Vacuum Packaging Design Process for Microelectromechanical System (MEMS) Quad-Mass Gyroscopes

by Rohan Deshmukh, Ryan Knight, and Dr William Nothwang

NOTICES

Disclaimers

The findings in this report are not to be construed as an official Department of the Army position unless so designated by other authorized documents.

Citation of manufacturer's or trade names does not constitute an official endorsement or approval of the use thereof.

Destroy this report when it is no longer needed. Do not return it to the originator.

ARL-TR-7825 ● SEP 2016

US Army Research Laboratory

A Novel Vacuum Packaging Design Process for Microelectromechanical System (MEMS) Quad-Mass Gyroscopes

by Rohan Deshmukh
Aerospace Engineering, Georgia Institute of Technology, Atlanta, GA

Ryan Knight and Dr William Nothwang
Sensors and Electron Devices Directorate, ARL

REPORT DOCUMENTATION PAGE

Form Approved
OMB No. 0704-0188

1. REPORT DATE *(DD-MM-YYYY)*	2. REPORT TYPE	3. DATES COVERED (From - To)
September 2016	Technical Report	05/2015–08/2016

4. TITLE AND SUBTITLE
A Novel Vacuum Packaging Design Process for Microelectromechanical System (MEMS) Quad-Mass Gyroscopes

5a. CONTRACT NUMBER

5b. GRANT NUMBER

5c. PROGRAM ELEMENT NUMBER

6. AUTHOR(S)
Rohan Deshmukh, Ryan Knight, and Dr William Nothwang

5d. PROJECT NUMBER

5e. TASK NUMBER

5f. WORK UNIT NUMBER

7. PERFORMING ORGANIZATION NAME(S) AND ADDRESS(ES)
US Army Research Laboratory
ATTN: RDRL-SER-L
2800 Powder Mill Road
Adelphi, MD 20783-1138

8. PERFORMING ORGANIZATION REPORT NUMBER
ARL-TR-7825

9. SPONSORING/MONITORING AGENCY NAME(S) AND ADDRESS(ES)

10. SPONSOR/MONITOR'S ACRONYM(S)

11. SPONSOR/MONITOR'S REPORT NUMBER(S)

12. DISTRIBUTION/AVAILABILITY STATEMENT
Approved for public release; distribution is unlimited.

13. SUPPLEMENTARY NOTES

14. ABSTRACT
Gyroscopes are an integral component of inertial measurement units. They are important to Army systems as they provide Soldiers with information on position, navigation, and timing. The majority of microelectromechanical system (MEMS) gyroscopes in production today are vibratory rate gyroscopes, making them resonant systems. Of the various systematic performance parameters for resonant systems, the quality factor (Q-factor) is an important measure. Q-factor for resonant MEMS such as the quadruple-mass gyroscope (QMG) strongly depends on the pressure at which the system operates. To improve upon Q-factor of the existing MEMS gyroscope, a novel submilliTorr vacuum packaging approach was designed. The packaging process has been broken down into systematic steps with the goal in each step to reduce internal packaging pressure, which was measured using commercial off-the-shelf Pirani gauges. The process was then tested on in-house fabricated QMGs, where Q-factor was measured for both short- and long-term stability. The packaging process will be valuable for improving MEMS gyroscope performance and pursuing further development.

15. SUBJECT TERMS
gyroscopes, vacuum packaging, hermetic sealing, Pirani gauge, residual gas analyzer

16. SECURITY CLASSIFICATION OF:			17. LIMITATION OF ABSTRACT	18. NUMBER OF PAGES	19a. NAME OF RESPONSIBLE PERSON
a. REPORT	b. ABSTRACT	c. THIS PAGE			Ryan Knight
Unclassified	Unclassified	Unclassified	UU	46	19b. TELEPHONE NUMBER (Include area code) (301) 394-3710

Contents

List of Figures

List of Tables

INTENTIONALLY LEFT BLANK.

1. Introduction/Background

There has been a growing need in society today for objects that humans use, both militarily and commercially, to be durable, faster, and efficient. From tanks and automobiles to unmanned aerial vehicles (UAVs) and robots, the need for improved performance is ubiquitous. Electronic sensors are no exception. In recent years, there has been a substantial amount of time and money invested in improving the performance and operability of position, navigation, and timing (PNT) systems. These systems need to be lighter, cheaper, and more power efficient to match the growing global dependence on them. In the defense sector, such devices should be able to match the various constraints and performance criteria of air and land robots, munitions, and constrained vehicle platforms. Currently, the standard navigation system that the US military uses is GPS. However, one of the drawbacks of GPS is its inherent weak signal and vulnerability to jamming by natural and unnatural means. This sole dependence on GPS technology may prove to be catastrophic if the signal is lost or broken. As such, development of microelectromechanical system (MEMS) inertial sensors that can provide navigation-grade performance can alleviate the military's reliance on a single PNT.

This report focuses primarily on improving the performance of one PNT system, a resonant quadruple-mass gyroscope (QMG), which has been manufactured in-house by the US Army Research Laboratory (ARL) in Adelphi, Maryland.

1.1 Overview of MEMS Gyroscopes

Gyroscopes are one of the most important position sensors out in today's market. A gyroscope is an in situ physical sensor that can detect and measure angular motion in an inertial reference frame. By being an in situ sensor, or measuring within itself, the gyroscope can measure absolute motion without relying on an external reference or signal. If 3 gyroscopes are combined with 3 accelerometers, another in situ physical sensor, a 6-axis inertial measurement unit (IMU) can be produced (Trusov 2011). A powerful PNT system, IMUs can be commonly found on most autonomous or intelligent systems, such as quadrotor helicopters and cell phones.

Gyroscopes are commonly divided into 3 categories: angle (or whole angle or rate integrating) and rate. Like the name suggests, angle gyroscopes measure absolute angular position. Similarly, rate gyroscopes measure absolute angular rates. The most common type of gyroscope being developed and manufactured today is the silicon vibratory rate gyroscope. An example of such a device is the ARL-fabricated QMG, shown in Fig. 1. The QMG was designed at the University of California,

Irvine under the Defense Advanced Research Projects Agency program. The design uses 4 silicon spring-suspended masses moving anti-phase from one another in the same plane of the chip to detect rotation angle out of plane of the chip (Trusov et al. 2014). What is unique about the device is that the QMG can not only operate as a rate gyroscope, but it has the capabilities to operate as a whole-angle device as well. Although in its infancy stages in performance determination and optimization, the potential for the QMG to be a powerful and efficient gyroscope is limitless.

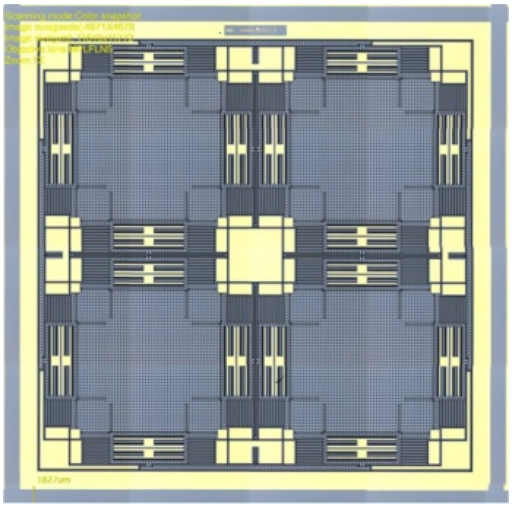

Fig. 1 ARL-fabricated QMG

In the past few decades, sensors and electronics have seen a rapidly diminishing form factor in terms of size. The current paradigm can be seen in MEMS becoming smaller, lighter, and faster. Physically, MEMS devices have a diminutive form factor ranging from 0.1 to 1,000 μm in any dimension. With the current trend in technology development, the future holds for devices to be manufactured within the nano regime, as seen in Fig. 2. However, if nanotechnology is indeed the technology of the future, then MEMS is the technology of today (Fan 1988).

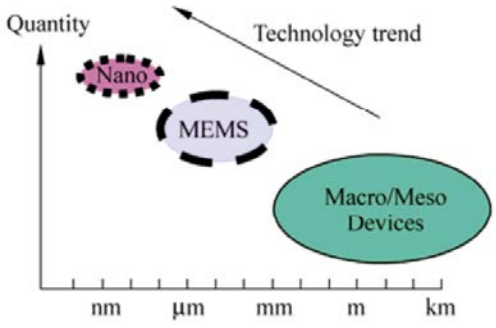

Fig. 2 Size of various devices following the technology trend

Evidently, MEMS technology has seen its infusion into gyroscopes, particularly silicon-based vibratory rate gyroscopes, due to strong ties with semiconductor technology. Due to their size, power requirements, and cost, MEMS gyroscopes have become a particular favorite in various motion-detecting applications, such as consumer electronics and automotive safety devices (Trusov 2011).

1.1.1 Performance Parameters

A simple analytical model of a single-axis vibratory rate gyroscope is shown in Fig. 3. A rate gyroscope operates with nonsymmetry between the drive mode and sense mode, the x and y axes, respectively. The drive mode is driven into forced vibration mode with a prescribed amplitude and angular frequency. The sense mode acts to suppress the driven vibrations and can be used to measure input rate (Trusov 2011). Through this vibration feedback, a MEMS gyroscope acts as a resonant system.

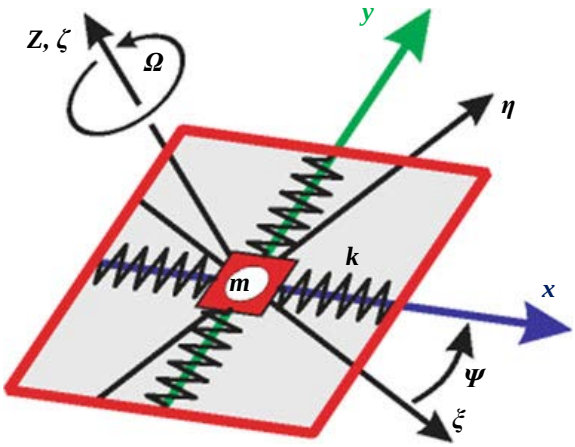

Fig. 3 Theoretical model of a single z-axis vibratory gyroscope

There are numerous systematic parameters that characterize MEMS gyroscope performance. These parameters include scale factor, bandwidth, bias, and quality factor (Q-factor). In particular, this report looks into ways of improving Q-factor through vacuum packaging.

Q-factor is arguably the most important performance parameter. As mentioned earlier, the amount of vibration transferred from the drive to sense axis is dictated by the Coriolis force produced. The Coriolis force and, hence, the amplitude of the sense axis vibration, is proportional to the rotation rate (Leland 2005). Furthermore, it is also directly proportional to the Q-factor of the mode-matched gyroscope as seen by Eq. 1:

$$y_{0_{matched}} = \Omega_z \frac{2Q_s x_o m_c}{m_s \omega_s}. \quad (1)$$

Q-factor is defined as the ratio between the amount of stored energy the gyroscope has to the amount of energy dissipated out per radian (Prikhodko et al. 2013). Ideally, the most efficient gyroscope would have a Q-factor of infinity, directly correlating to zero dissipated energy. However in reality, it is impossible to achieve such value. The benefit of high Q-factors is improved noise resolution and higher measurement sensitivity. Thus, when a PNT platform requires high precision and accuracy, high Q-factor gyroscopes are needed.

To look at the importance of Q-factor to package pressure, it is important to analyze the empirical equation governing Q-factor, represented by Eq. 2 (Kim, et al. 2006):

$$\frac{1}{Q_{total}} = \frac{1}{Q_{air}} + \frac{1}{Q_{TED}} + \frac{1}{Q_{anchor\ loss}} + \frac{1}{Q_{other}}. \tag{2}$$

For a packaged system in a moderate vacuum pressure, if we assume thermal elastic dissipation to be negligible and ignore anchor loss and other, Eq. 2 can be simplified to

$$\frac{1}{Q_{total}} \approx \frac{1}{Q_{air}}. \tag{3}$$

Air damping can be modeled for these microscale resonating structures by Eq. 4, which can be approximated to be proportional to square root of temperature over package pressure as seen by Eq. 5:

$$Q_{air} = \frac{h\left(\frac{\pi}{2}\right)^{2.5} \rho f \sqrt{\frac{k_b T}{m}}}{p}. \tag{4}$$

$$Q_{air} \propto \frac{\sqrt{T}}{p}. \tag{5}$$

If temperature is fixed, it can be seen by linking Eq. 5 with Eq. 4 that low package pressures will result in high total Q-factors.

1.2 Vacuum Packaging Overview

Packaging is one of the most important and expensive steps in the life cycle of MEMS manufacturing. On average, packaging takes up between 30%–70% of the total manufacturing cost. In terms of functionality, the purpose of packaging is to protect, power, and cool microelectronic chips or components while providing mechanical and electrical connections to the outside world. Furthermore, many MEMS packages require additional considerations such as a hermetic seal and vacuum encapsulation (Chiao et al. 2002). For MEMS gyroscopes, these additional requirements are warranted as a device's performance increases in a vacuum

environment and the resonator does not want to be exposed to a phenomenon known as stiction due to high concentrations of moisture.

With the general demand of high-performance gyroscopes, the industrial trend over the past few decades is finding ways to improve vacuum packaging performance. Figure 4 illustrates this trend linking systematic performance parameters of Q-factor and bias with manufacturing cost for various industry demand regimes (Prikhodko et al. 2013). Although the most precise gyroscopes are the most expensive, future trends in vacuum packaging design will have substantially lower costs with very little loss in performance.

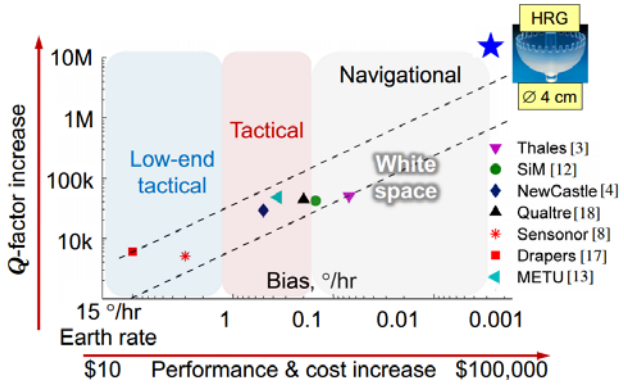

Fig. 4 MEMS gyroscope performance vs. cost tradeoff

1.2.1 General Packaging Procedure

There are numerous MEMS gyroscope packaging procedures in the scientific community. Although each procedure was developed for a unique piece of hardware, all share the same common engineering strategy when it comes to vacuum packaging. Figure 5 depicts a block diagram of the overall packaging procedure.

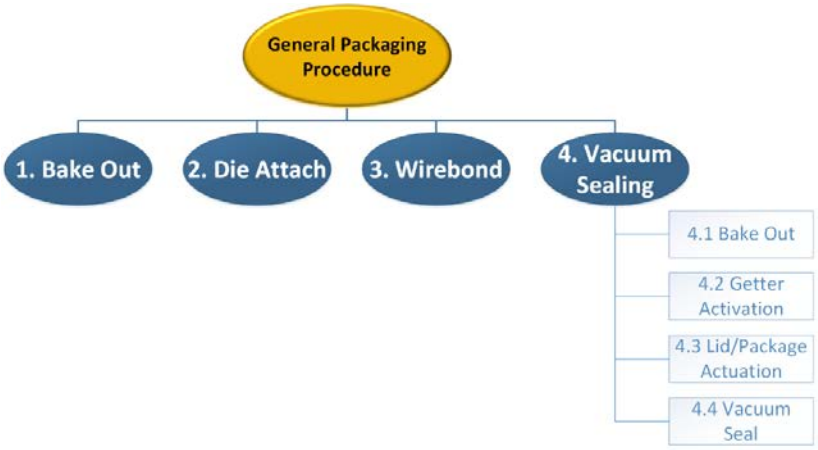

Fig. 5 Overall MEMS vacuum packaging procedure

1.2.1.1 Bake Out

Bake out is the first step in any packaging sequence, although it does not happen during vacuum packaging itself. The goal here is to remove any residual species that might become trapped inside of package. For example, a significant amount of hydrogen can become trapped in the electroplated metal coating on the package, making the package itself a major source of outgassing (Schofield et al. 2010). The general practice used to remove potentially trapped species is to bake out the package in a high-temperature and ultra-high vacuum environment. An example of such can be a 1-h bake out at 400 °C and 1×10^{-6} Torr.

1.2.1.2 Die Attachment

After baking out the package, the MEMS die itself must be attached to the package. The die can be attached using a solder preform or an adhesive such as Kapton tape. The goal here is to provide a strong bond between the package and die with little stress and as little potential for outgassing as possible. An example solder preform used is 80/20 gold (Au)-tin (Sn) due to its low eutectic melting temperature of 280 °C and its low outgassing properties. An example die attach schematic is shown in Fig. 6.

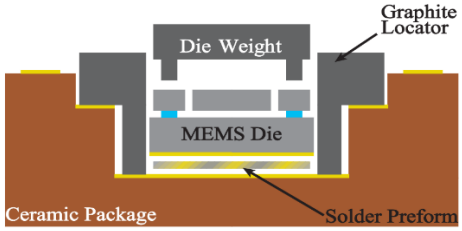

Fig. 6 Example die attachment schematic

1.2.1.3 Wirebond

In order for the MEMS die to connect electrically with the package or other electrical devices inside of the package, the die must be wirebonded to the respective component. Typically, an industrial wirebonder is used in order to produce precise and low-stress attachment points with either ball, wedge, or compliant bonding types. The bond wires are always metals and can range from aluminum to Au composition. An example wirebond can be seen in Fig. 7 where the MEMS die is connected to the package itself.

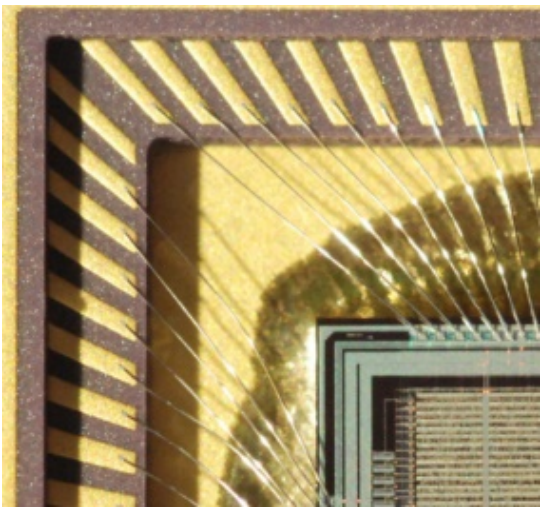

Fig. 7 Example wirebond between MEMS die and package

1.2.1.4 Vacuum Sealing

Vacuum sealing is the final step in the packaging process. The goal here is to ensure the lid bonded to the package provides a hermetic, airtight seal. Before the final seal is attached, all components must go through a final bake out to remove any residual species that may have been introduced during die attachment and wirebonding steps. In order to fully remove these species, a specifically designed getter will need to be activated in order to absorb and remove them. Depending on what types of species need to be removed, different getter materials are chosen. For example, a getter made out of a desiccant or polymer material will target and remove moisture from the package. The polymer will form hydrates when reacting with water and will act as a quasi-pump when drying out the package. To transition to the sealing stage, the lid must be lowered and aligned properly with the package. Finally, the lid is bonded directly to the package by melting of the preform. Similar to the die attach preform solder, 80/20 Au-Sn is widely chosen as the lid preform material. Figure 8 show a post-packaging sealing where the sealing lid is the last component added in the packaging process

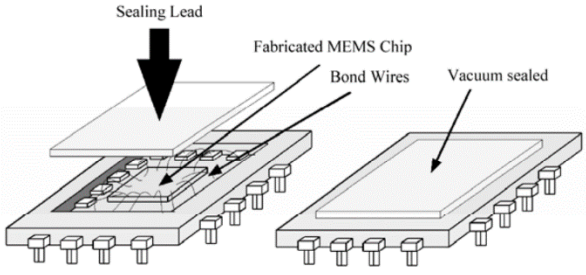

Fig. 8 Post-packaging vacuum lid seal

1.3 Pirani Gauge Overview

For MEMS gyroscopes, maintaining a proper hermetic seal is vital for both the performance and longevity of the device. The seal is maintained through the monitoring of the internal package pressure. Typical monitoring techniques include a helium leak rate test as well as pressure extracted from the Q-factor. Although these accepted techniques do provide insight into status of hermetic seal, they require a laborious test setup and expensive equipment, and cannot observe minute changes in pressure. Another cost-effective and efficient method is using Pirani gauges. These Pirani gauges provide in situ measurements of internal package pressure without compromising the integrity of the seal through destructive testing. They are manufactured small enough to fit into virtually any package and can be placed in an array setup to provide a high-resolution measurement of the package pressure.

Pirani gauges are suspended resistors in which heat loss provides a measure for the surrounding pressure (Santagata et al. 2010). Typically, Pirani gauges specific for MEMS applications are manufactured to operate in a variety of low-pressure environments (Topalli et al. 2009). Figure 9 illustrates the basic fundamentals on how a Pirani gauge operates.

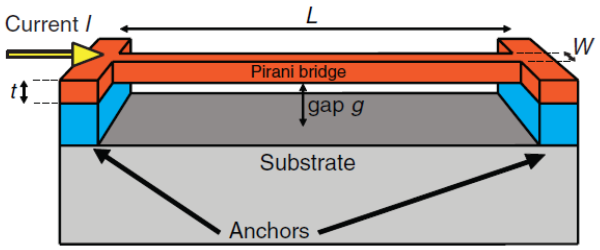

Fig. 9 Physical components of MEMS Pirani gauge

When a current, I, is applied to the gauge and passes through the bridge, the temperature of the gauge increases; thus, the resistance changes. As the temperature increases, heat is transferred, conductively and convectively, from the bridge to the substrate via anchors and gas within the gap g. As the pressure of the Pirani gauge changes, the conductance of the gas changes as well. This can be easily seen through the definition of thermal conduction. Since resistance is defined as the inverse of conductance, if the conductance of the gas changes, the resistance of the Pirani gauge would change as well. Thus, the measurement of voltage across the bridge of the Pirani gauge is a direct indication of pressure. This relationship can be simply modeled by Ohm's Law:

$$V(p) = IR(p). \tag{6}$$

There have been theoretical models developed for Pirani gauges that try to expand upon the simple relationship outlined by Eq. 6. In general, any expansion done will leave the equation transcendental in nature. To overcome this, transfer functions are required. For simplicity, this report does not use an analytical model for determining package pressures, but uses calibration curves to determine pressure given a voltage reading. Both approaches generate voltage versus pressure curves that are S-shaped in nature. Figure 10 illustrates a sample analytical model and Fig. 11 illustrates a manufacturer-tested Pirani gauge calibration curve.

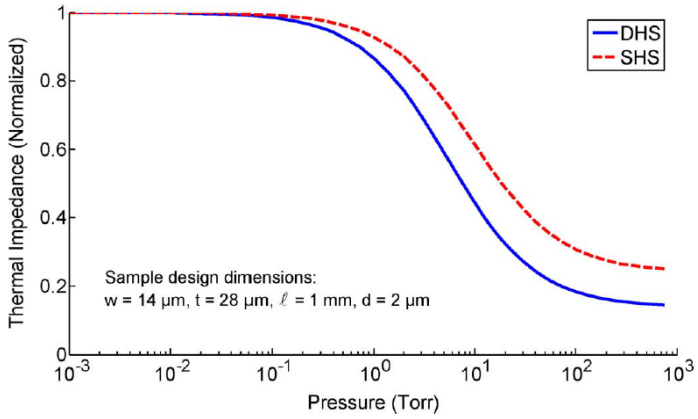

Fig. 10 Sample Pirani gauge pressure vs. voltage model

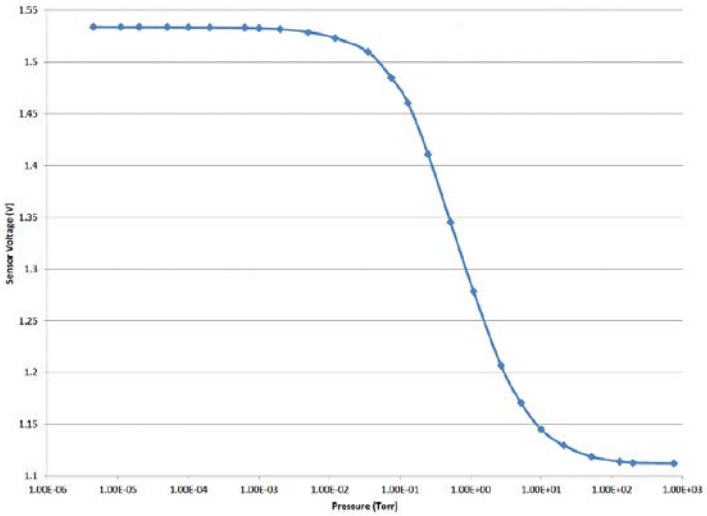

Fig. 11 Manufacturer-produced pressure vs. voltage graph

2. Experimental Approach

To achieve the engineering goal of improving QMG performance through a novel vacuum packaging process, the complete packaging process was analyzed and

dissected into 3 main categories: in situ pressure gauging, heating design, and outgassing analysis. Each category has the same theme in mind: finding ways to accurately determine pressure and reduce it. Within each of the 3 categories, a series of experiments was conducted that directly correlated and contributed to the universal theme. These experiments were designed based on an extensive literature review on the subject of vacuum packaging.

2.1 Thermal Fluctuation Experiment

Thermal fluctuation is defined as the perturbation a thermodynamic system undergoes from its equilibrium state. Generally, thermal fluctuation is primarily influenced by temperature as a gradient of temperature acting on a system can cause perturbation to that system both macro- and microscopically. For Pirani gauges, keeping a steady temperature is essential for accurate measurements of pressure through voltage readings. When testing in a lab environment, it is very hard to control the ambient room temperature as there are a plethora of heat sources and sinks within the laboratory itself. The physical effect of thermal noise on a Pirani gauge can be seen in the change in conductance. Through Fourier's Law for 1-D thermal conductance, the local heat flux can be related to the differential in temperature scaled by the material's thermal conductivity by Eq. 7 (DeWitt and Incropera 1953):

$$q_x = -k\frac{dT}{dx}. \tag{7}$$

If Eq. 7 is integrated around the gauge's surface area, A, and the gauge is assumed to be composed of homogenous material, uniform k, one can obtain Eq. 8:

$$\frac{\Delta Q}{\Delta t} = -kA\frac{\Delta T}{\Delta x}. \tag{8}$$

We can tie Eq. 8 to conductance through its relationship with resistance. From Pouillet's Law, Eq. 9, electrical resistance is proportional to electrical resistivity, ρ, of the gauge and length of bridge, x, while inversely proportional to the bridge's cross-sectional area, A:

$$R = \rho\frac{x}{A}. \tag{9}$$

By definition, electrical conductance, G, is defined as the inverse of electrical resistance and can be written as

$$G = \frac{1}{R} = \frac{kA}{x}. \tag{10}$$

For heat transfer, conductance, U, can be written in a similar form as Eq. 10:

$$U = \frac{kA}{\Delta x}. \tag{11}$$

Substituting Eq. 11 into Eq. 8 and simplifying using inverse relationship between conductance and resistance, a simple relationship between temperature and heat transfer per unit time can be generated:

$$R = \frac{\Delta T}{\dot{Q}}. \tag{12}$$

For temperature fluctuations across the Pirani gauge, the resistance of the gauge changes accordingly. Applying Ohm's Law, one can see that a change in pressure coupled with a constant prescribed current will cause changes in voltage measurements across the gauge. As a result, thermal noise is added to the voltage readings, thus making the task of precisely measuring pressure onerous. One possible solution to this problem is directly controlling the temperature in a temperature chamber. However, due to the immobility of such a device, it does not provide a flexible solution to mitigating thermal fluctuations. Instead, a widely practiced routine used by Pirani gauge manufacturers is a Wheatstone bridge configuration.

Bridge circuits are the most common method of connecting passive transducers to measuring systems. One of the most widely implemented bridge circuits is the Wheatstone bridge configuration devised by SH Christie in 1833 (Beckwith et al. 1995). An example of a DC Wheatstone bridge configuration is shown in Fig. 12.

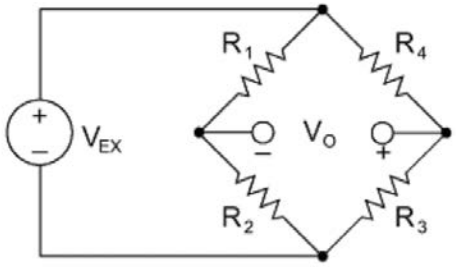

Fig. 12 Sample Wheatstone bridge circuit configuration

Typically, one or more of the resistors, shown in Fig. 13, are of unknown value and through the balancing of the bridge, $v_o = 0\ V$, the value can be determined. For a Pirani gauge, the goal of a Wheatstone bridge configuration is to shunt temperature-induced resistance fluctuations and allow for more accurate measurements of the gauge voltage. Using a voltage-feedback loop connected to the bridge, the

resistance of one of the known legs can be fine-tuned to nullify gauge resistance perturbation and maintain a balanced bridge.

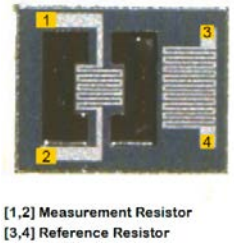

Fig. 13 Die connections for a PTCD10 resistor

For this experiment, a thermal gas conductivity sensor die PTCD10, manufactured by Posifa Microsystems Inc., was used as the pressure sensor. Although not an integrated Pirani gauge with a bridge configuration, the die was chosen due to its diminutive size and its ability to be wirebonded to the package itself. The die consists of 2 thermally dependent resistors, as shown by Fig. 12. The reference resistor allows for reference of an on-chip voltage change, which directly correlates to a temperature such that the pressure change can be thermally isolated.

When designing the Wheatstone bridge setup for the PTCD10, it was important to note that 2 legs of the bridge, the measurement resistor and the reference resistor, would need to be shunted to remove thermal fluctuations from the voltage measurements. Furthermore, the shunting would require a differential resistor; thus, potentiometers were implemented. The circuit diagram that was implemented during testing is shown in Fig. 14 and the actual setup is shown in Figs. 15 and 16.

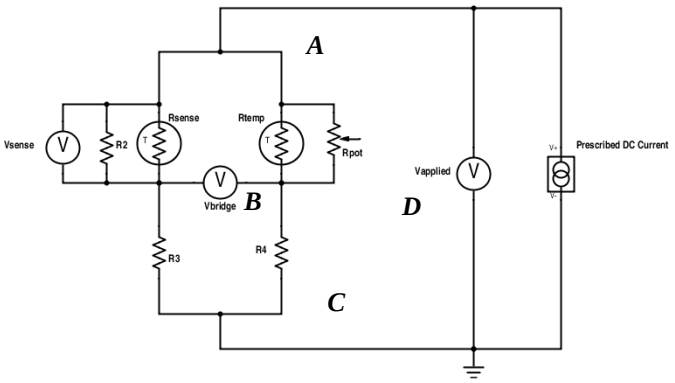

Fig. 14 Wheatstone bridge test: circuit diagram

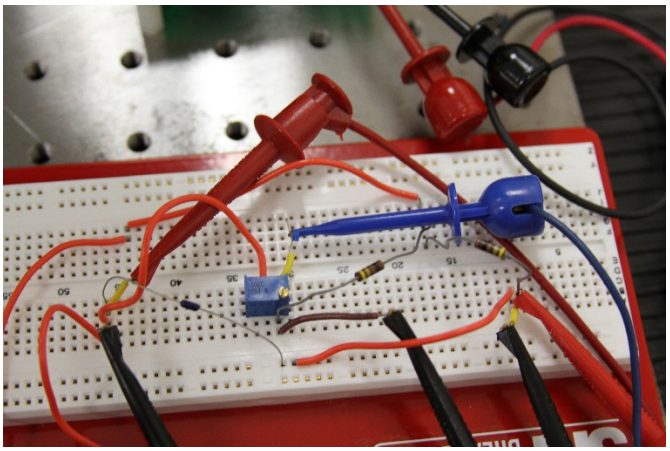

Fig. 15 Wheatstone bridge test: breadboard implementation

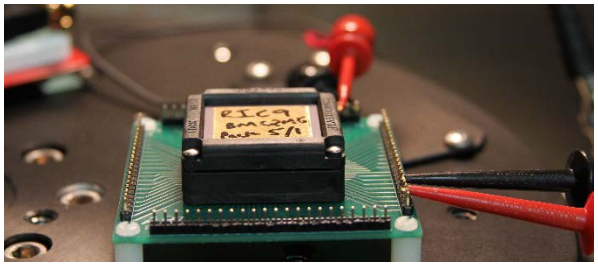

Fig. 16 Wheatstone bridge test: test package in temperature chamber

Three voltmeters ($V_{applied}$, V_{bridge}, V_{sense}) were used to measure the voltage across the entire setup, the bridge, and the measurement resistor, respectively. A DC constant-current bridge approach was implemented, instead of a DC constant-voltage bridge, to regulate current throughput through the die. The current through each leg can be determined using Kirchoff's current divider law. The resistance values of R_2 and R_{pot} were chosen based on a sensitivity analysis of ΔV_{ac}, where the goal was to make $\Delta V_{ac} \rightarrow 0\ V$ given $R_3 = R_4$, $\Delta R_3 = \Delta R_4 = \Delta R$, and $V_{bd} = 0\ V$. Equation 13 shows the mathematical sensitivity of ΔV_{ac} and Eq. 14 shows the theoretical value for R_{pot} to maintain a balanced bridge:

$$V_{ac} + \Delta V_{ac} = \frac{I\left(\frac{1}{R_{pot}} + \frac{1}{R_{temp}+\Delta R}\right)^{-1}}{\left(\frac{1}{R_4} + \frac{1}{R_{sense}+\Delta R}\right)^{-1} + \left(\frac{1}{R_{pot}} + \frac{1}{R_{temp}+\Delta R}\right)^{-1}} \left(\left[\frac{1}{R_4} + \frac{1}{R_{sense}+\Delta R}\right]^{-1} + R_3\right). \quad (13)$$

$$R_{pot} = \left[\frac{1}{R_4} + \frac{1}{R_{sense}} - \frac{1}{R_{temp}}\right]^{-1}. \quad (14)$$

The test setup consisted of a temperature chamber that was set to 4 static room temperature values: 15, 20, 25, and 30 °C. The current source was set to a range of values (15, 25, 35, 45, 55, and 65 mA) that prescribed between 2–10 mA through

the measurement resistor. Based off sensitivity analysis, the resistors were chosen to be $R_2 = 50\ \Omega$, $R_3 = R_4 = 100\ \Omega$, and $R_{pot} = 40\ \Omega$. The potentiometer was calibrated initially at 15 °C, 15 mA and stayed static throughout experiment. The result of the experiment is shown in Fig. 17. Table 1 highlights the prescribed current values through the measurement resistor, theoretical potentiometer resistance, and percent error from the static potentiometer value.

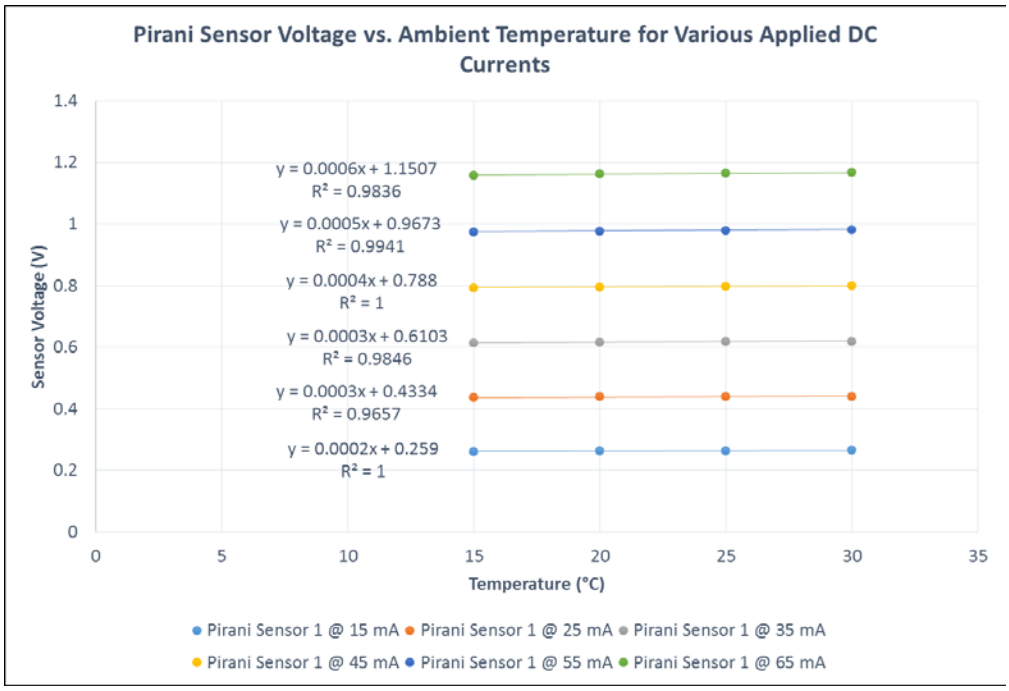

Fig. 17 Thermal fluctuation experiment results

Table 1 Data output from Wheatstone bridge experiment

Temp (°C)	DC current (mA)	I_{sense} (mA)	R_{pot} (theoretical) (Ω)	% error (R_{pot})
15	15	2.185	40.712	0.52%
	25	3.645	40.712	0.52%
	35	5.129	40.712	0.52%
	45	6.622	40.712	0.52%
	55	8.132	40.712	0.52%
	65	9.666	40.712	0.52%
20	15	2.168	40.796	0.73%
	25	3.619	40.796	0.73%
	35	5.087	40.796	0.73%
	45	6.562	40.796	0.73%
	55	8.063	40.796	0.73%
	65	9.588	40.796	0.73%
25	15	2.153	40.870	0.91%
	25	3.589	40.870	0.91%
	35	5.041	40.870	0.91%
	45	6.509	40.870	0.91%
	55	7.993	40.870	0.91%
	65	9.502	40.870	0.91%
30	15	2.139	40.937	1.07%
	25	3.559	40.937	1.07%
	35	5.004	40.937	1.07%
	45	6.457	40.937	1.07%
	55	7.934	40.937	1.07%
	65	9.427	40.937	1.07%

From the results, it can be seen that the Wheatstone bridge setup produces an ideal shunting of temperature-induced voltage fluctuations across the measurement resistor of the PTCD10 die. The slope of the plots generated in Fig. 17 shows that at best the bridge setup can guarantee a stable, unhindered voltage reading of ±0.2 mV per 1 °C fluctuation. Furthermore, with increasing applied current, the voltage reading sensitivity increases slightly but is small in comparison with voltage sensitivities without the bridge configuration. Table 1 suggests that swapping a static 40-Ω resistor with a potentiometer will provide sufficient resistance to balance the bridge as there is a less than 1% error in potentiometer resistance. Nevertheless, the Wheatstone bridge design will provide for more precise measurement of the Pirani gauge voltage values and thus allow for more accurate characterization of the internal package pressure.

2.2 Heating Profile Design

Heating profile is at the center of the packaging process. It defines the physical process for which a package is hermetically sealed in a vacuum environment. A heating profile is a temperature versus time plot of the complete packaging process and is typically produced by a packaging machine. An example heating profile that outlines the major packaging steps can be seen in Fig. 18 (Prikhodko et al. 2013). A well-designed heating profile can make the difference between a moderate pressure package and an ultra-low vacuum package.

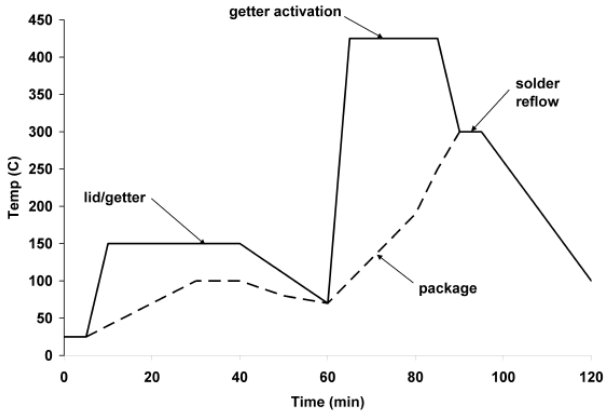

Fig. 18 Sample heating profile for high vacuum sealing

The heating profile designed that this report discusses was created using Suss SB8e wafer bonder manufactured by Suss Microtech. The bonder was set up for preform eutectic bonding with a transport fixture that allows for spacer/clamp actuation. The system uses a graphical user interface (GUI) that allows the operator to create the heating profile, or what Suss calls “recipe creation”. An example recipe for Au-Sn wafer bonding is shown in Fig. 19.

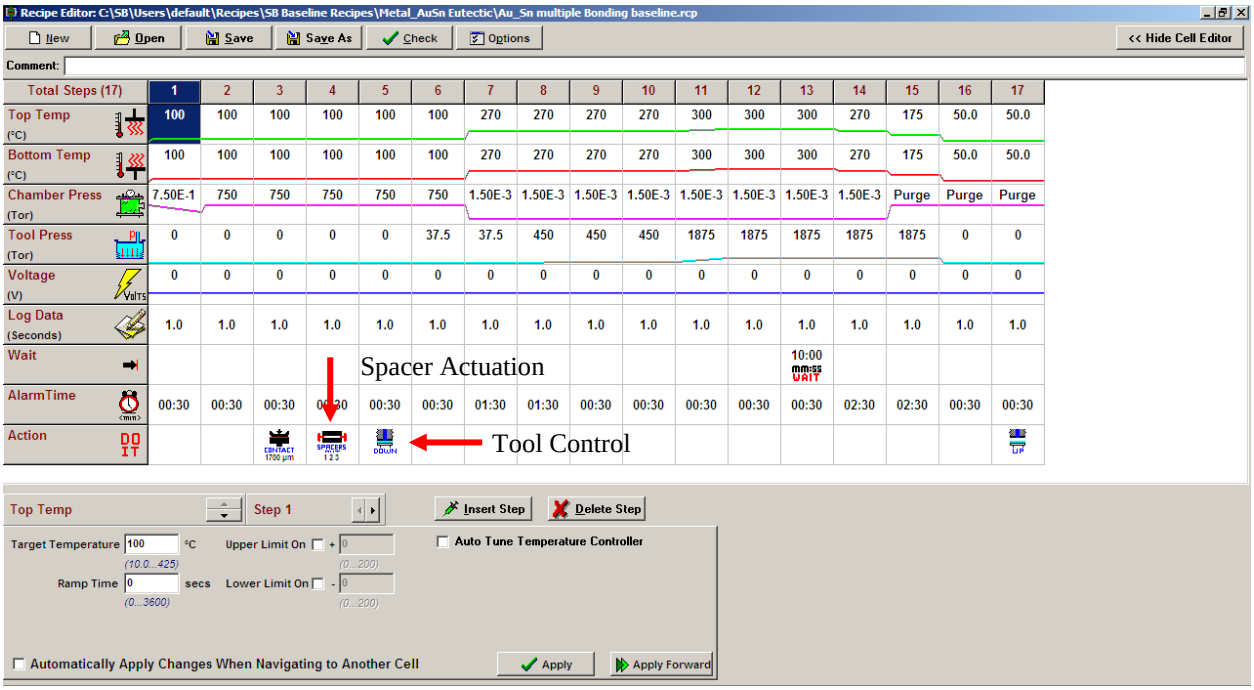

Fig. 19 Sample Suss SB8e recipe for Au-Sn eutectic bonding

As shown in Fig. 19, the recipe editor allows for numerous system parameters to be controlled, including temperature of the top and bottom heating plates, chamber pressure, tool pressure, spacer/clamp/tool actuation, log time, and wait time for each step.

As outlined in Section 1.2.1, the heating profile was designed based off the 4 main steps of vacuum packaging. Each step begins with a baseline approach found from literature review on the subject, and through iteration, the step is optimized until desired performance is achieved, as shown by Fig. 20.

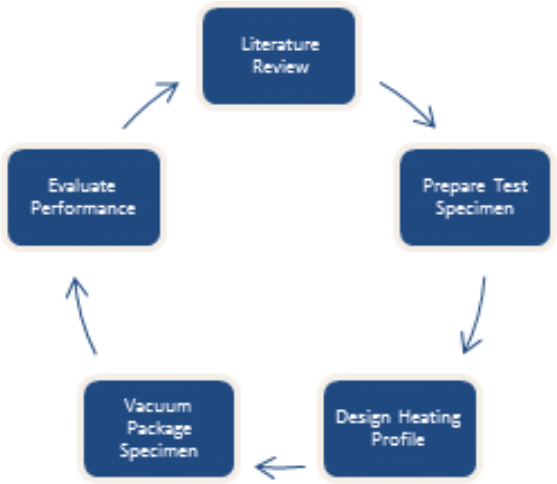

Fig. 20 Heating profile design iterative process

It is important to note that these baseline approaches are not universal to all vacuum packaging systems and are directly dependent on what system is being used. It only provides guidance or a starting point to where testing on a Suss machine should begin. The primary materials used in the heating profile design, excluding the Suss-manufactured parts, are listed in Table 2.

Table 2 Heating profile design test specimens

Component name	Material info
Ceramic package	Kyocera A-440 (sapphire [Al_2O_3]), electroplated nickel (Ni) and Au
Lid	Kovar, electroplated Ni and Au
Preform	80/20 Au-Sn
Superglue	Ethyl cyanoacrylate
PTCD10 die	Pirani gauge
QMG	Silicon-based

2.2.1 Bake Out

A substantial amount of literature provide various recommendations for bake-out schematics. The general range of bake-out temperatures in a vacuum environment for eutectic bonding goes from as low as 50 °C to as high as 400 °C (Paquet et al. 2013). One of the primary concerns with low-temperature bake outs (50–200 °C) is the time required to drive out trapped hydrogen gas in electroplated lid and package, which is on the order of weeks to months. On the other side of the spectrum, a temperature higher than 350 °C is needed in order to drive hydrogen from iron-based alloys. Although the bake-out time is substantially reduced, a consequence of the high temperature is a reduction in wire bondability due to surface Au diffusion and reaching the preform's eutectic point. It is suggested that an optimized bake out be done at 250 °C for 1 week to nullify evolved hydrogen concentrations. However, empirical data suggests that a bake out at 400 °C for 1 h without the preform attached to the lid provides similar results (Ramesham 2004).

Using these 2 aforementioned suggestions, tests were conducted to determine which setup would yield to a lower package pressure. Due to onerous suggested time of 1 week (168 h), the 250 °C bake-out temperature was tested at 48 and 72 h, trials 1 and 2, respectively, initially in order to determine if increasing bake-out time does lead to lower package pressures. These tests were conducted with the package, lid, and preform, where spacers were implemented to displace the preform and lid from the package. Table 3 outlines the results from the experimentation, which shows that increasing time duration at 225 °C did improve internal package pressure, but not substantially.

Table 3 Suss SB8e package bake-out experimentation results

Trial no.	Components	Temperature (°C)	Chamber pressure (Torr)	Duration (h)	Package pressure (Torr)
1	Lid + preform, package	225	4.E-05	48	20
2	Lid + preform, package	225	4.E-05	72	18
3	Package	400	4.E-05	1	6
	Lid + preform, package	225		48	

In order to test the 1-h, 400 °C suggestion, trial 3, the package needed to be baked out separately from the lid and preform to avoid the preform's eutectic point. Furthermore, using a similar setup as the previous 2 trials, the package was rebaked with the lid and preform after tests for wire bondability were conducted. The results shown in Table 3 along with residual gas analyzer (RGA) readings not only confirm the empirical data suggestion, but provide insight into the importance of baking components separately initially before vacuum-seal bake out, as seen by the substantial reduction in package pressure.

From these trials, the final bake-out parameters for testing on packaging a QMG were determined as shown in Table 4. The parameters are almost identical to trial 3 with the addition of baking out the lid separately. The result of this addition is a considerable reduction in package pressure to 3 Torr. Due to time constraints, more testing and optimizing of bake-out parameters could not be accomplished. However, the preliminary results from the bake-out design provide important insight into what parameters drastically improve packaging pressure as it moves into the desired submilliTorr regime.

Table 4 Suss SB8e bake-out parameters used to obtain package pressure of 3 Torr

Heating profile step	Components	Temperature (°C)	Chamber pressure (Torr)	Duration (h)	Package pressure (Torr)
Bake-out	Package	400	4.E-05	1	3
	Lid + preform	225		12	
	Lid + preform , package	400		48	

2.2.2 Ramp-Up

Ramp-up is the step where entire package suite is heated from its bake-out temperature to a maximum heating profile temperature, typically greater than the preform's eutectic melting temperature. The goal of this step is to ensure the eutectic temperature of the preform is reached while setting up the lid for bonding with the package. A ramp-up can be accomplished either linearly, by setting the end temperature and allowing the bonding system to reach it on its own, or

piecewise, where the operator defines temperature values to be met and steps up to the end temperature. One of the most important driving factors for the designed ramp-up's performance is heat transfer. In a low-vacuum environment, the most dominant type of heat transfer is radiation. Radiation heat transfer between 2 objects can be modeled by Stefan-Boltzmann equation, Eq. 15, where Q is the heat flux, ε is the emissivity of the object, σ is Stefan-Boltzmann constant, and T is the temperature of the object:

$$Q = \varepsilon\sigma\left({T_1}^4 - {T_2}^4\right). \tag{15}$$

For a perfect blackbody, $\varepsilon = 1$; however, in most cases, the material used in vacuum packaging will have a $\varepsilon < 1$. As a result, the only mathematical way to transfer a lot of energy in the form of heat from body 1 to body 2 is to have body 1 be as hot as possible and body 2 be as cool as possible. Relating this to the ramp-up design, the maximum heating profile temperature will need to be substantially larger than the preform's eutectic melting temperature in order to guarantee the preform melting in an ultra-low-vacuum environment.

To have more user control over the ramp-up, a piecewise approach was implemented in the experimentation. During the beginning of the ramp-up, spacers were actuated to lower the lid and preform onto the package and a wafer bonder tool was lowered to provide weight on the lid. Using the aforementioned bake-out temperature, the Suss SB8e was programmed to reach a maximum temperature of 425 °C in an ultra-low-vacuum environment. Through iteration, the value of a 425 °C was chosen to provide consistent eutectic melting and adequate time for the preform to reflow and solidify. In general, it was determined that temperatures above 400 °C were needed to reach the 278 °C eutectic temperature of 80/20 Au-Sn. Table 5 outlines the ramp-up parameters used to obtain a package pressure of 3 Torr

Table 5 Suss SB8e ramp-up parameter used to obtain a package pressure of 3 Torr

Heating profile step	Max temperature (°C)	Chamber pressure (Torr)	Temperature intervals (°C)	Duration (min)
Ramp-up	225	4.E-05	300, 350, 375	6

2.2.3 Lid Seal

Physically, lid seal is the point where the preform reaches its eutectic point, melts into liquid form, and bonds through solidification via reflow onto the package. One important consideration for lid sealing is bonding time. It is important to provide adequate time above the preform's eutectic point to ensure proper bonding between

the package and the lid. If not enough time is given, the preform may not reflow enough to provide a hermetic seal and thus compromise the integrity of the vacuum package. An example of a poor bond is shown in Fig. 21, where the result of the bond was a complete loss in vacuum pressure of the package despite the preform melting to the package.

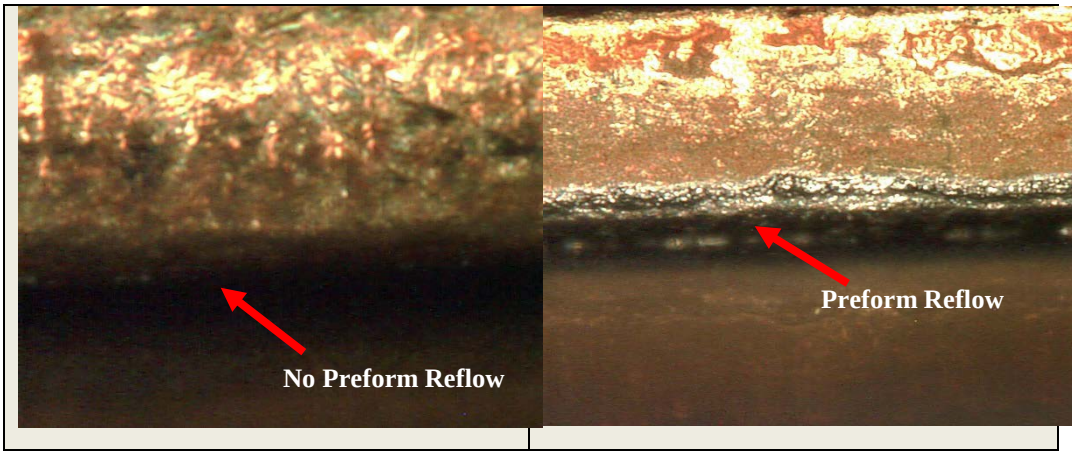

Fig. 21 Optical photograph of a poor and good preform bond

The designed lid seal operates at 425 °C in a vacuum environment and was held for 10 min to ensure, at a minimum, at least 5 min above the experimental testing melting temperature of the preform in Suss SB8e, namely, 400 °C. Figure 22 is the temperature output from the Suss SB8e for the lid sealing step, which validates that the minimum time-above-eutectic was satisfied. Table 6 outlines the lid seal parameters used to obtain a package pressure of 3 Torr.

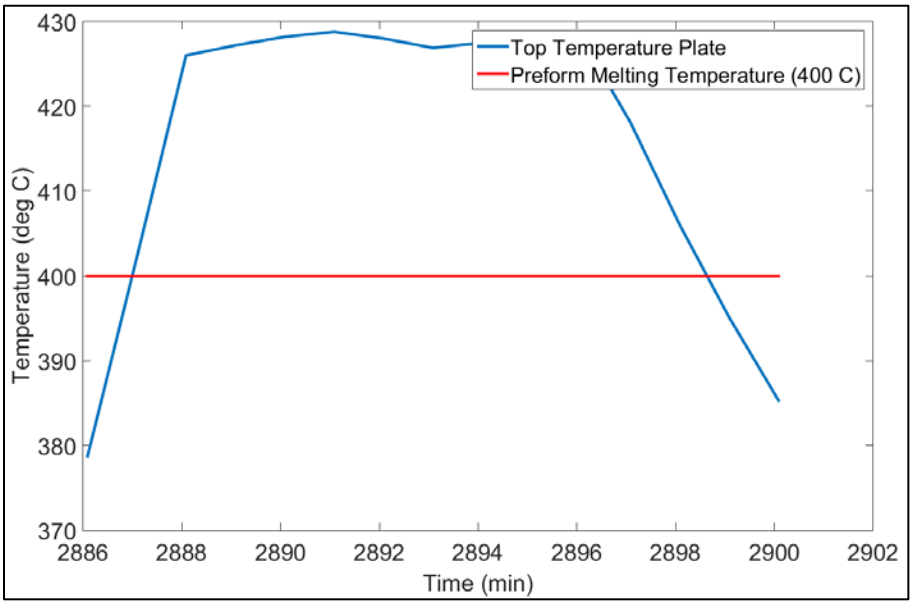

Fig. 22 Suss SB8e temperature profile for the lid sealing phase

Table 6 Suss SB8e lid seal parameter used to obtain a package pressure of 3 Torr

Heating profile step	Temperature (°C)	Pressure (Torr)	Duration (min)
Lid seal	425	4.E-05	10

2.2.4 Cool/Purge

The goal of cooling is to ensure proper reflow of the preform as it transitions from a liquid to a solid state and ensure proper cooling of the system in a low-vacuum environment. Like the ramp-up stage, cooling can be accomplished linearly or piecewise. Furthermore, to improve heat transfer, low nitrogen gas can be purged into the system (Prikhodko et al. 2013).

To have more user-control over cooling, a piecewise approach was implemented in the experimentation. The system was gradually brought down in temperature while still in a low-vacuum environment. To prepare the package for removal, the wafer bond tool was actuated up and the system was purged. Table 7 outlines the cool/purge parameters used to obtain a package pressure of 3 Torr.

Table 7 Suss SB8e cool/purge parameter used to obtain package pressure of 3 Torr

Heating profile step	Min temperature (°C)	Pressure (Torr)	Temperature intervals (°C)	Cooling duration (min)	Purge duration (min)
Cool/purge	25	4.E-05	200, 150, 50	20	30

Through the iterative process in the heating profile design shown in Fig. 19, a consistent and repeatable vacuum packaging process was produced. The resulting package from the heating profile design is at a low pressure and is hermetically sealed. In addition, the implementation of spacers in the design sequence proved to be substantial in the performance of the design. Figure 23 depicts the overall heating profile design used to achieve a 3-Torr package pressure.

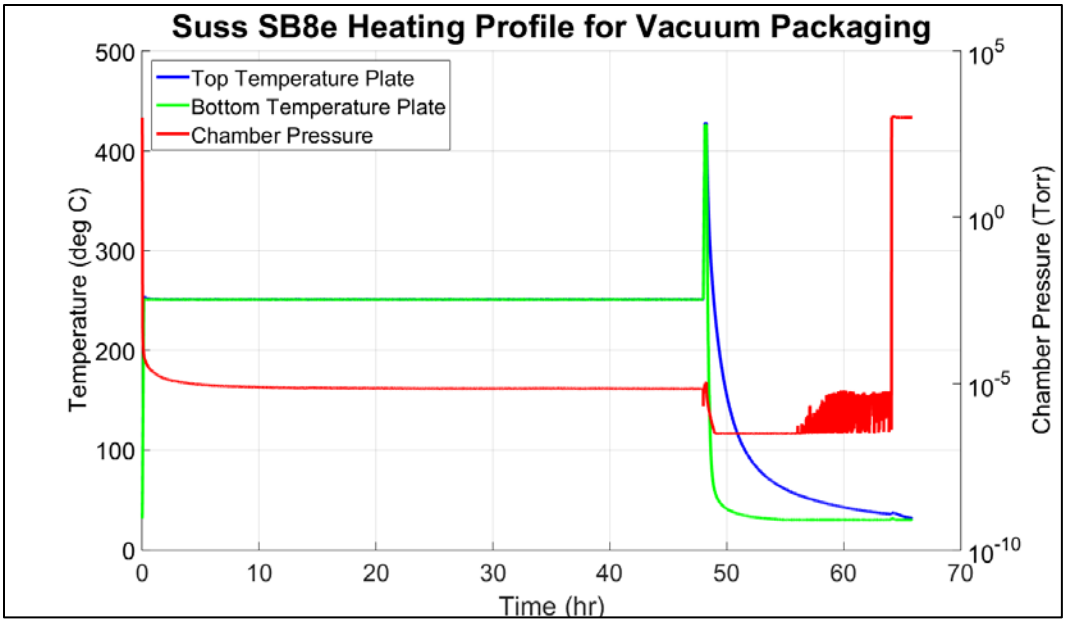

Fig. 23 Overall Suss SB8e heating profile for submilliTorr vacuum packaging

2.3 Residual Gas Analyzer Experiment

The motivation behind vacuum packaging is not just centered on improving MEMS performance. One of the critical roles vacuum packaging has is providing internal component safety and longevity. A proper hermetic seal will allow for MEMS devices to be thermodynamically isolated from the ambient operating environment. This, in turn, reduces any potential for life-time degradation of the device. It is also important to remove any outgassed or residual species from the package before it is sealed. Similarly, a proper vacuum package will negate any potential for harmful species to interact with the device. In view of the latter point, an RGA experiment was conducted in order to analyze outgassing and residual species during the heating profile design and provide insight into outgassing mitigation techniques.

An RGA is a small, rugged mass spectrometer used in process control and contamination-monitoring of vacuum systems. It is used in most cases to measure the quality of the vacuum and can measure extreme vacuums as low as 10^{-14} Torr. An RGA works on the principle of mass-to-charge ratios where a small fraction of incoming gas molecules are positively ionized and the resulting ions are separated, detected, and measured according to their molecular mass (Stanford Research Systems 2009).

For this experiment, the Pfeiffer Prisma 80 QME-200 RGA was hooked up to a pressure-tap valve on the Suss SB8e wafer bonder as shown in Fig. 24. A manual control-valve was also installed to control the vacuum pressure going to the RGA

as the specific RGA implemented can operate in vacuum conditions of 1×10^{-4} mbar (7.5×10^{-5} Torr) or less. The materials used in the experimentation were the same as materials used in the heating profile design. Additionally, a literature review was conducted on component-specific materials and their key outgassing properties in high-temperature vacuum environments. These chemical properties were used as quality checks for the experiment. The list of test components and their outgassing properties are listed in Table 8.

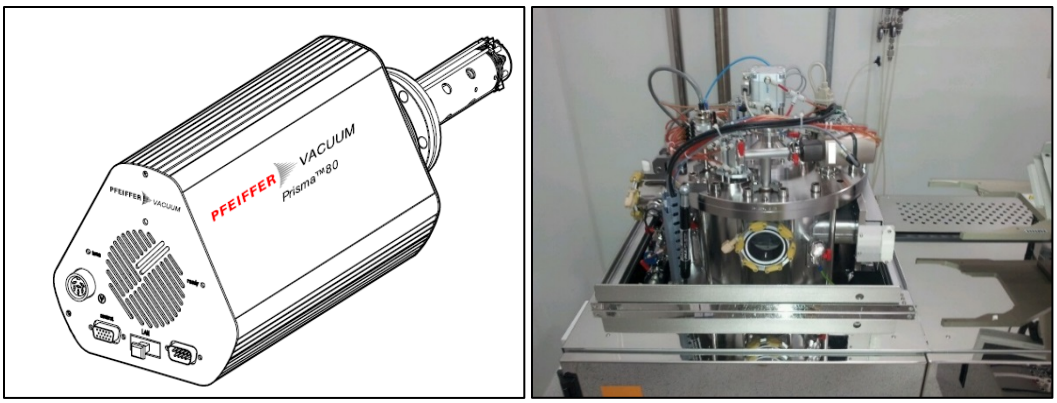

Fig. 24 RGA experiment setup

Table 8 RGA experiment test specimens and outgassing properties

Component name	Material info	Outgassing properties
Ceramic package	Kyocera A-440 (Al_2O_3), electroplated Ni and Au	Low CTE, traps H_2 and moisture
Lid	Kovar, electroplated Ni and Au	Traps H_2 and moisture
Preform	80/20 Au-Sn	Release CO_2 when melting
Superglue	Ethyl cyanoacrylate	Releases NO_x, CO, CO_2 when heated
PTCD10 die	Pirani gauge	N/A
QMG	Silicon-based	N/A

The results for the experiment not only validate the outgassing properties for each component, but provides insight into the major species present during the vacuum sealing process. During the bake-out step of the heating profile design, the primary species the RGA read was water vapor, as shown by Fig. 25. Water vapor is arguably one of the hardest molecules to remove from any vacuum system. Despite only constituting a minute concentration of around 4% in air at 1 atm and 20 °C, water vapor contributes a 7 Torr partial pressure and is dependent on the humidity levels of the air (Ramesham 2004). Through opening and closing the vacuum system door, the vacuum became exposed to ambient air and thus water vapor was reintroduced into the system. At low-pressure environments, water vapor becomes the dominant species in terms of partial pressure. The polar nature of water

molecules not only causes them to adhere to surfaces with weak bonds, but adhere to one another, thus creating layers of collected moisture (Danielson 2001). For a 1-h bake out, the readings indicate that the increasing concentrations of water come from trapped moisture outgassed from the electroplated package itself. Furthermore, the expected high concentration of water initially is a direct indication of the importance of baking out the vacuum chamber to remove residual layers of moisture before the heating profile can commence.

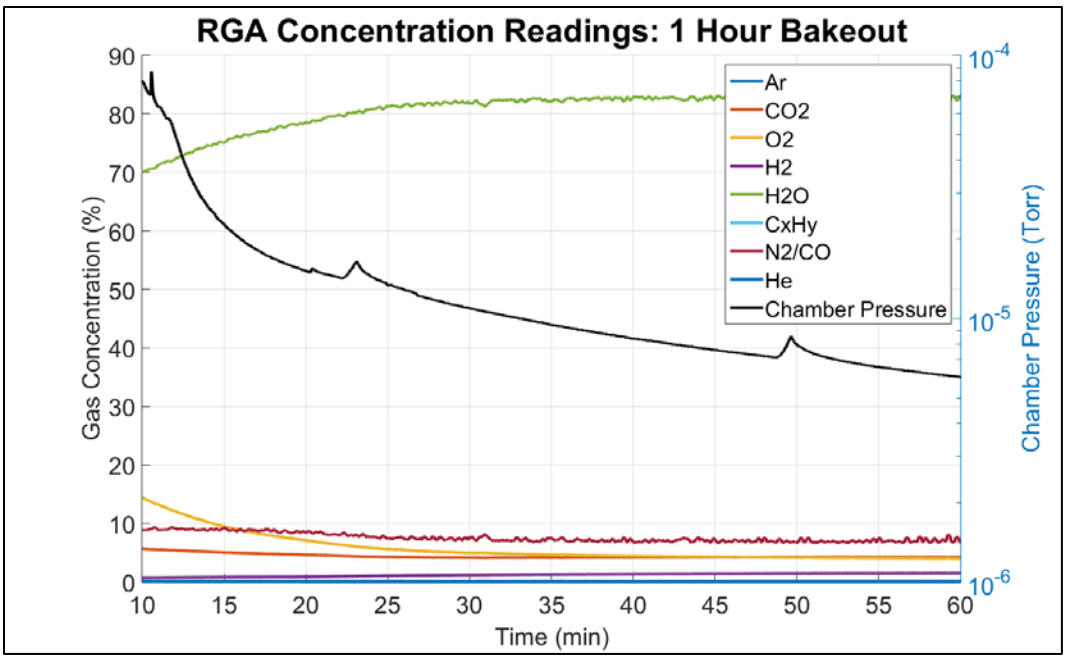

Fig. 25 RGA output for a 1-h bake out at T = 225 °C

To reduce these water concentrations over time, a longer bake out is needed. As shown by Fig. 26, an 8-h bake out is sufficient to drive down water concentrations as measured by RGA.

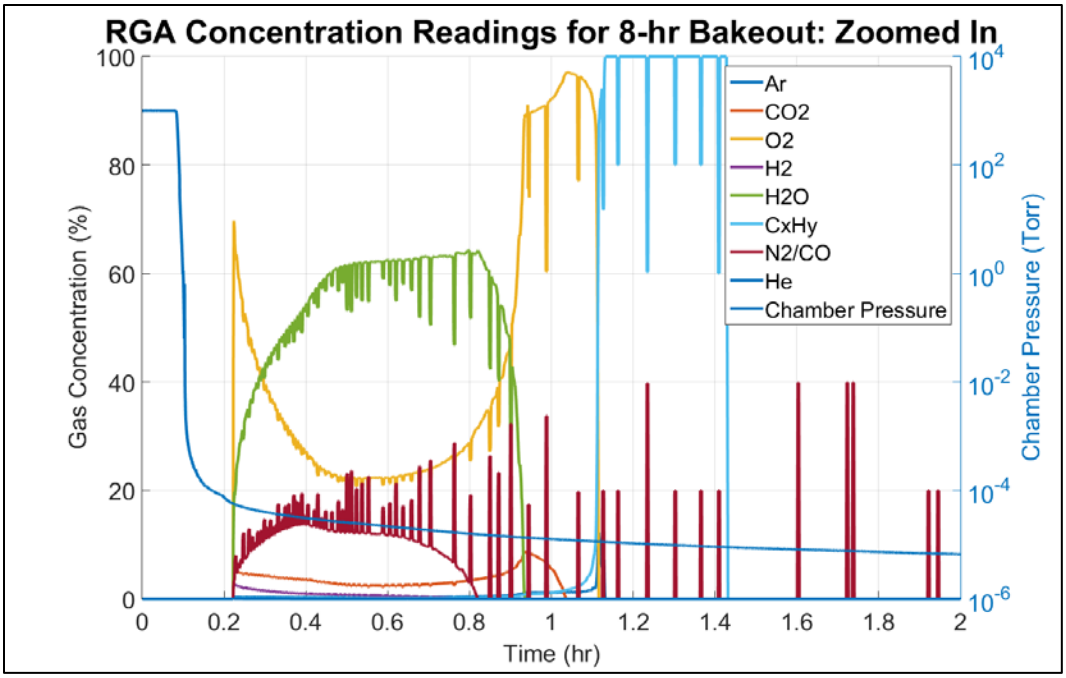

Fig. 26 RGA output of a 2-h sample for an 8-h bake out

The average H_2 concentration for an 8-h bake out was measured to be 0.0306%, which indicates the need for even longer bake outs to reduce H_2 concentration levels. Literature indicates bake outs on the order of 2–7 days at 250 °C are sufficient to reduce H_2 concentration levels. Nevertheless with a 48-h bake-out test conducted in the heating profile design, the average H_2 concentration was measured to be 0.00013%. This reduction in evolved hydrogen confirms the bake out's performance in removing trapped H_2 in the electroplated lid and package.

The presence of CO_2 was noted during the eutectic melting of the preform. As in any combustion reaction with excess oxygen, CO_2 is always a product. Figure 27 shows this phenomenon through the increase in CO_2 and the reduction in O_2.

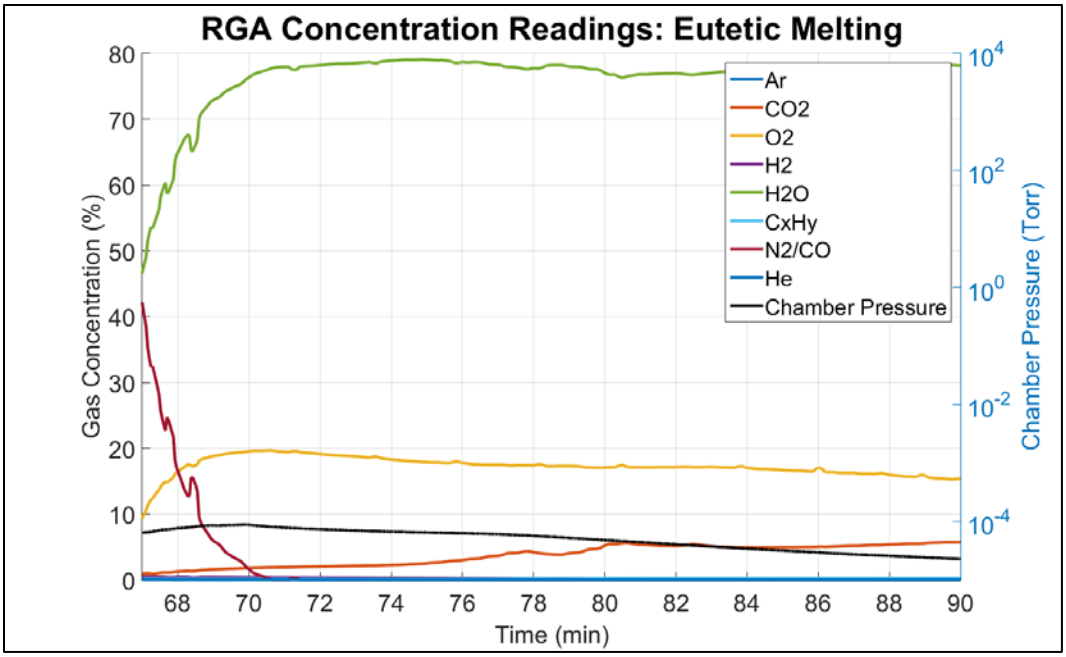

Fig. 27 RGA output of preform melting

Lastly, the RGA was able to confirm the outgassing of inorganic molecules (CO_2, CO, NO_x) from the heating of the superglue used to tack the PTCD10 die to the package. For the test depicted in Fig. 28, an excess amount of superglue was implemented. The result was a consistently elevated concentration of approximately 15% throughout the test duration. In actual implementation, not as much superglue would be implemented to bond the Pirani gauges. However, the key finding that this experiment demonstrates is the high outgassing from superglue. As ethyl cyanoacrylate is heated, it vaporizes very quickly into various organic molecules and compounds. Therefore, these compounds must be mitigated through an extensive bake out to avoid being trapped inside the sealed package. An alternative adhesive to superglue would be using Kapton tape. The tradeoff to using Kapton tape is although it has minute and negligible outgassing properties at elevated temperatures, it loses adhesive strength with increasing temperatures, thus increasing the potential for the Pirani gauge to become disconnected from the package surface, making wirebonding tedious.

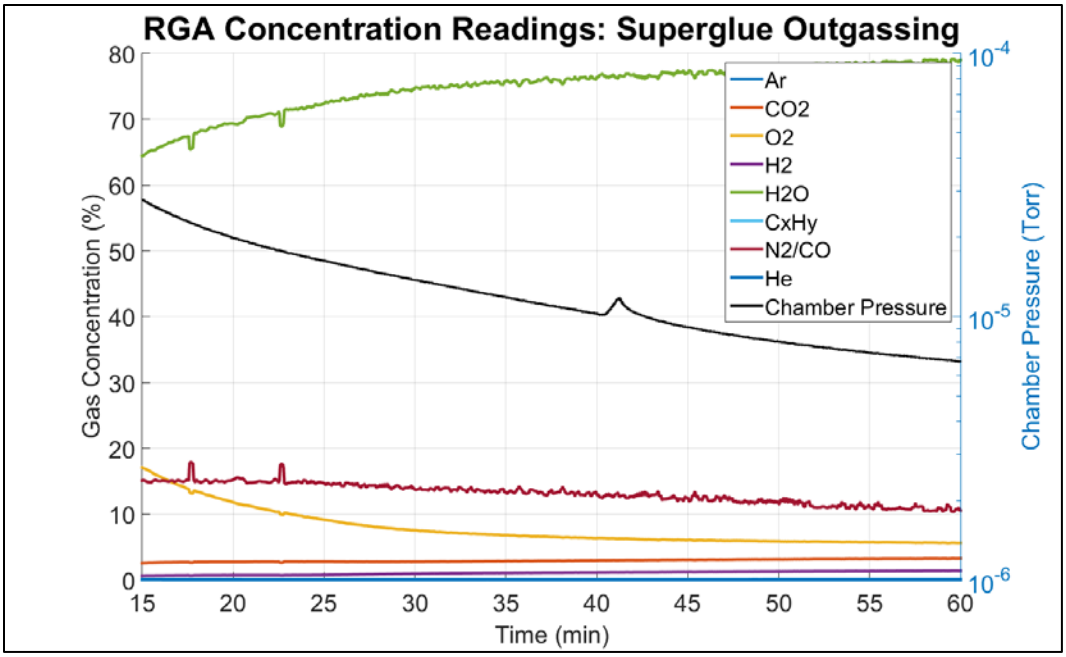

Fig. 28 RGA output of heating superglue

In summary, the RGA output provides good insight into the physical chemistry that occurs during the heating cycle. Although this work does not deal with getter activation, the data will allow for a better selection of getter material. Furthermore, the reduction of residual species over time serves as a qualitative check on the designed heating profile steps as well as the packaging material selection. It was found through experimentation that the reduction in key trapped species directly correlated to reductions in internal package pressure.

3. Results

The design methodology to measure Q-factor was centered on a frequency response of the gyroscope. For a resonating device such as a gyroscope, Q-factor is defined as the ratio of the resonant frequency, f_R, to the half-power bandwidth, Δf, as shown by Eq. 16. A frequency response of the gyroscope will allow for both the resonant frequency and bandwidth to be determined.

$$Q = \frac{f_R}{\Delta f}. \tag{16}$$

The gyroscope used throughout the entire vacuum packaging design and Q-factor determination was an in-house manufactured QMG, shown in Fig. 1. An experimental setup, as shown in Fig. 29, was created to conduct the frequency response.

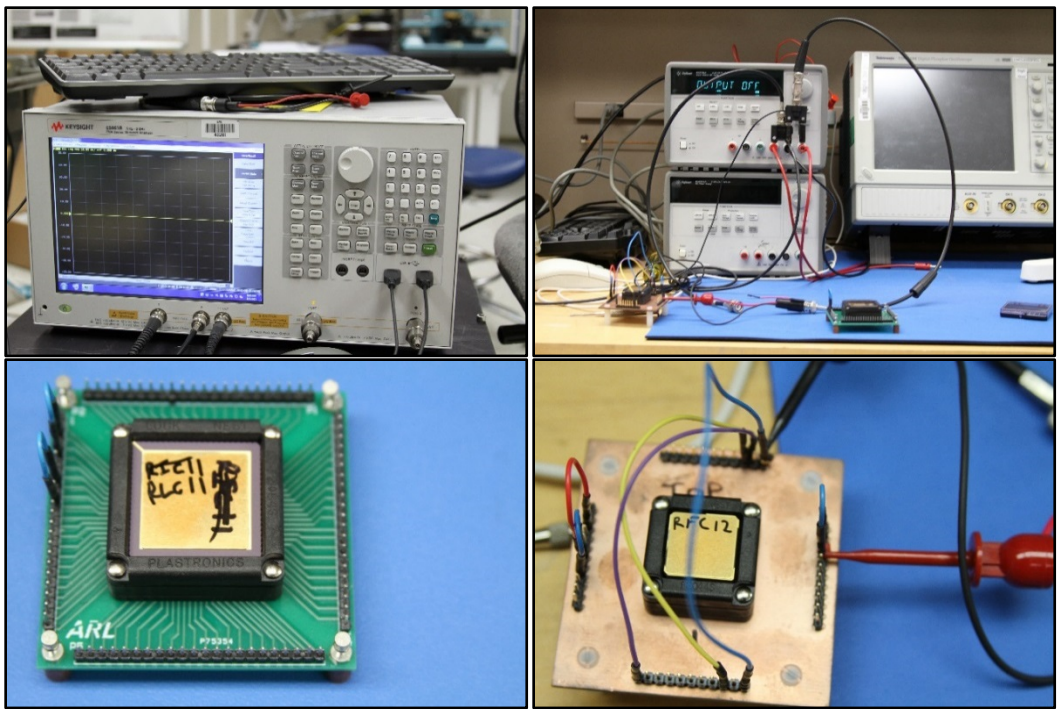

Fig. 29 Q-factor determination: experimental setup

An analog network analyzer was implemented (top left image of Fig. 29) to serve as the function generator for the prescribed signals for the drive mode (x-axis) and sense mode (y-axis). In addition, the network analyzer was also set up to measure the frequency response spectrum of both modes and output the data for postprocessing Q-factor determination. Lastly, a DC power supply (top right image of Fig. 29) was additionally implemented to prescribe a DC voltage/current to the QMG capacitors.

Q-factor for 2 QMGs were measured after vacuum packaging using the aforementioned experimental setup. One QMG, labeled RFC-12 in the bottom right image of Fig. 29, was previously packaged using an SST International 3130 Vacuum Furnace with a known internal package pressure of 40 Torr. The RFC-12 QMG served as a baseline/control for comparison with Suss SB8e vacuum packaged QMGs. Nevertheless, the other QMG, labeled RLC-11 in bottom left image of Fig. 29, was packaged in the Suss SB8e using foundations laid down in Section 2 with an internal package pressure of 3 Torr. The frequency response showing the resonant frequency, bandwidth, and Q-factor for each QMG with their respected measured package pressure is shown in Figs. 30 through 32.

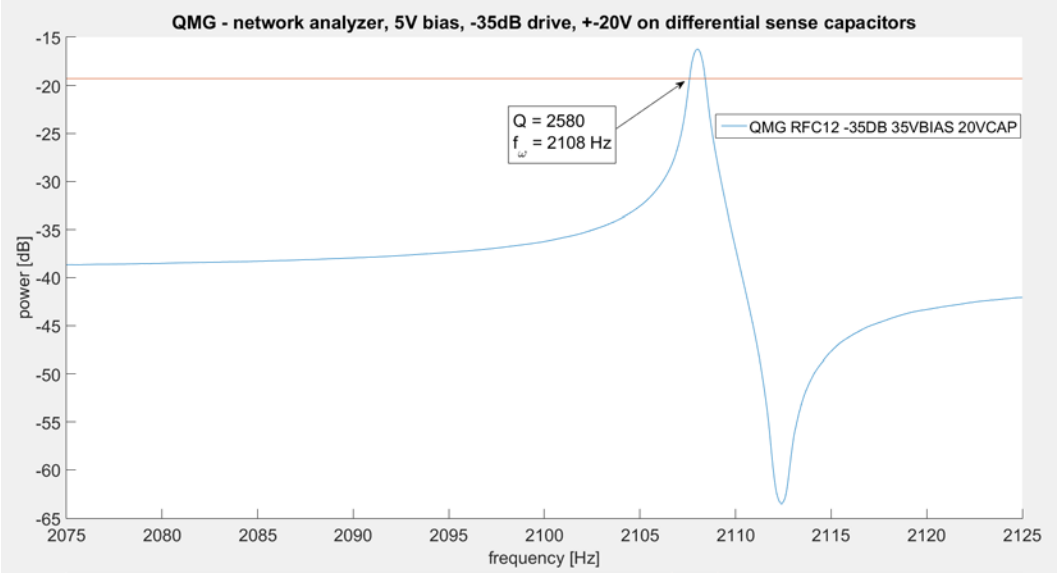

Fig. 30 Q-factor drive and sense mode: RF-C12 at 40 Torr

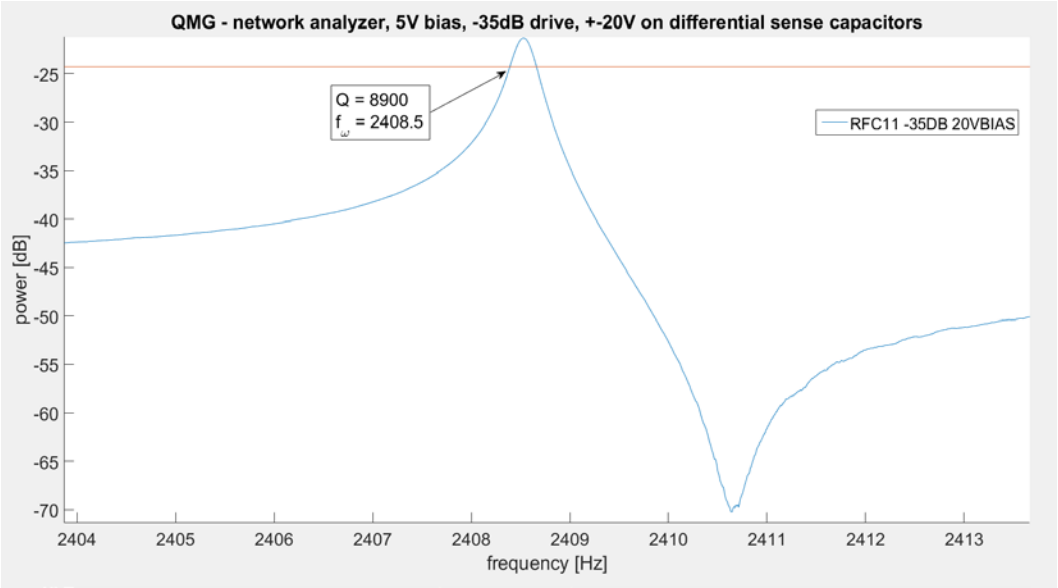

Fig. 31 Q-factor drive mode: RL-C11 at 3 Torr

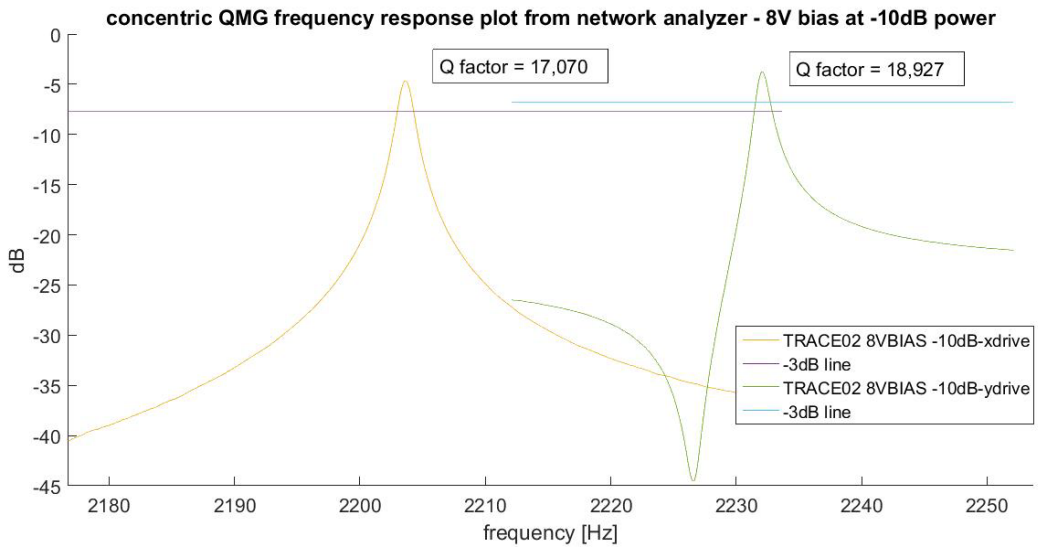

Fig. 32 Q-factor drive mode: RL-C11 at 100 mTorr

As expected, it can be seen that reductions in package pressure from 40 to 3 Torr directly correlate to significant increases in the gyroscope's Q-factor from 2,580 to 8,900. When packaging pressure was reduced to 100 mTorr, the resulting Q-factor was approximately 19,000. Furthermore, as expected, Q-factor calculated for the drive and sense modes of each package are nearly the same. Due to time limitations, this report was not able to expand this trend to ultra-low-vacuum packaged QMGs. However, future development expanding on this trend is expected to show relationships between Q-factor and package pressure, as seen by Fig. 33. ARL results are superimposed on Fig. 33 and Q-factors are slightly higher at the same pressure than the QMGs used in Prikhodko et al (2013). ARL's higher Q-factor is due to Prikhodko et al. (2013) use of a 100-µm-thick device layer, whereas the ARL QMGs are 40 µm thick. The thicker device layer will have higher squeeze film damping values and hence lower Q factor values.

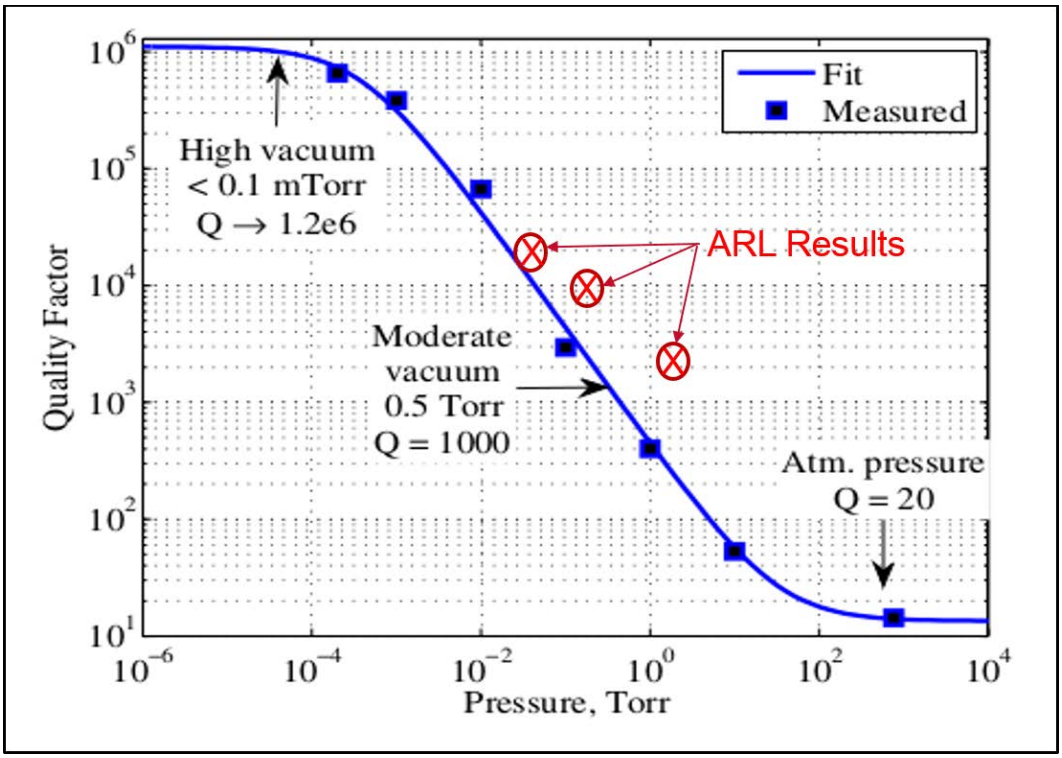

Fig. 33 Empirical relationship between quality factor and pressure for QMG (Prikhodko et al. 2013)

4. Conclusions

The overall motivation for designing a novel vacuum packaging design process was to improve a MEMS QMG's performance, in particular, its Q-factor. Through mathematical analysis and a literature review of Q-factor, it can found that Q-factor has a strong dependence on its operating environment's pressure. By linking pressure to Q-factor, a series of experimental approaches were conducted with the goal of finding ways to accurately determine pressure and reduce it. Finally, to truly validate this relationship, Q-factor for the QMG was determined.

The results show that importance of vacuum packaging for MEMS gyroscopes should not be overlooked. A properly designed heating profile can allow for a low packaging pressure to be obtained. The internal chemistry during the heating profile can be monitored using an RGA and, at the same time, can provide insight into performance of the heating profile and hermetic sealing. Although this report was unable to reach the packaging pressure goal of the submilliTorr regime, the data obtained from RGA will provide recommendations for future development such as the selection and implementation of getter material and cryogenic cooling to remove trapped water vapor inside the vacuum chamber. Through implementing an in situ approach while mitigating state function dependence, precise measurements

of internal vacuum pressure can be obtained. Putting all of these intertwined blocks together, the foundation of better-performing MEMS gyroscopes can be built.

5. Future Work

Despite the novel vacuum packaging process that was developed for the MEMS QMG in this report, there are various other experiments that need to be conducted to complete the overall vacuum packaging cycle. Future work will look into methods of expediting the heating profile design time while ensuring the same or improved performance. Based off preliminary RGA data, getter material can be selected and introduced into the packaging procedure. Secondly, through the RGA data, it was concluded that the reason the developed heating profile was unable to generate submilliTorr packaging pressures was due to residual water vapor trapped inside the package. As residual water vapor is a major problem in a vacuum system, future tests will be conducted with the goal of removing trapped moisture from the vacuum system. Finally, tests will be conducted on the heating profile itself to make it universal to industrial vacuum systems.

The long-term stability of a hermetically sealed package is important for the lifetime of the packaged device. The vacuum packaging process developed provides the foundation for fabricating a hermetic seal. Future work will build upon this foundation and test for its long-term performance through helium leak-rate tests that can be set to meet a certain minimum criterion. Furthermore, long-term stability of the seal will directly lead to long-term stability of the gyroscope's Q-factor. As such, future work will also test packaged QMGs for their Q-factor days, weeks, and months after the completed packaging process.

Other performance parameters of gyroscopes, such as bias stability and angle random walk, can be improved through a proper, stable vacuum package. As these gyroscopes with inevitably operate in dynamic environments, a proper packaging process must be developed to ensure long-term durability while increasing performance. Future work dealing with these other performance parameters will be conducted as well.

6. References

Beckwith T, Marangoni R, Lienhard J. Mechanical measurements. 5th edition. New York (NY): Wiley; 1995. Vol 7, p. 272–281.

Chiao M, Lin L. Technical digest of solid-state sensor. Actuator and Microsystems Workshop, Hilton Head, SC, 2002 Jun; p. 81–85.

Danielson P. The effects of humidity on vacuum systems. R&D Magazine; 2001.

DeWitt D, Incropera F. Introduction to heat transfer. New York (NY): Wiley; 2002. Vol. 2, p. 52–72.

Fan L, Tai Y, Muller R. Integrated movable micromechanical structures for sensors and actuators. IEEE Trans Electron Devices. 1988;35(6):724–730.

Kim B, Jha C, White T, Candler R, Hopcroft M, Agarwal M, Park K, Melamud R, Chandorkar S, Kenny T. Temperature dependence of quality factor in MEMS resonators. In: Proceedings of the IEEE International Conference on Micro Electro Mechanical Systems (MEMS); 2006 Feb;17:590–593.

Kyocera. Material properties; n.d. [accessed 2015 Jul]. http://global.kyocera.com/prdct/semicon/material/.

Leland R. Mechanical-thermal noise in MEMS gyroscopes. IEEE Sensor J. 2005;5(3).

Paquet A, Deshaies S, Desroches Y, Whalin J, Topart P. Influence of ceramic package internal components on the performance of vacuum sealed uncooled bolometric detectors. Proc SPIE. 2013.

Permabond. Material safety data sheet. Pottstown (PA): Permabond; 2006.

Prikhodko I, Simon B, Sharma G, Zotov S, Trusov A, Shkel A. High and moderate-level vacuum packaging of vibratory MEMS. Irvine (CA): University of California, Irvine; 2013.

Ramesham R, Evaluation of non-evaporable getters for high vacuum hermetic packages. Pasadena (CA): Jet Propulsion Laboratory, California Institute of Technology; 2004.

Santagata F, Iervolino E, Mele L, van Herwaarden A, Creemer J, Sarro P. An analytical model and verification for MEMS Pirani gauges. Delft (Netherlands): Delft University of Technology; 2011.

Spectrum Semiconductor Materials, Inc. SSM P/N LCC08423. San Jose, CA; n.d.

Stanford Research Systems. Operating manual and programming reference: models RGA100, RGA200, and RGA300 Residual Gas Analyzer. Sunnyvale (CA): Stanford Research Systems; Rev 1.8; 2009.

Topalli E, Topalli K, Alper S, Serin T, Akin T. Pirani vacuum gauges using silicon-on-glass and dissolved-wafer processes for the characterization of MEMS vacuum packaging. IEEE; 2009.

Trusov A. Overview of MEMS gyroscopes: history, principles of operation, types of measurements. Irvine (CA): University of California, Irvine, CA; 2011.

List of Symbols, Abbreviations, and Acronyms

ARL	US Army Research Laboratory
COTS	commercial off-the-shelf
Q-factor	quality factor
DC	direct current
GPS	global positioning system
IMU	inertial measurement unit
MEMS	micro-electro-mechanical systems
PNT	positioning, navigation, and timing
QMG	quadruple-mass gyroscope
UAV	unmanned aerial vehicle

1 (PDF)	DEFENSE TECH INFO CTR DTIC OCA
2 (PDF)	US ARMY RSRCH LABORATORY IMAL HRA MAIL & RECORDS MGMT RDRL CIO LL TECHL LIB
1 (PDF)	GOVT PRNTG OFC A MALHOTRA
2 (PDF)	CERCOM A SCHOFIELD P OLSON
2 (PDF)	RDECOM AMRDEC B GRANTHAM T HUDSON
7 (PDF)	US ARMY RSRCH LAB RDRL SE K KAPPRA RDRL SER L B PIEKARSKI RDRL SER L G L SMITH RDRL SER L J CONROY RDRL SER L R KNIGHT RDRL SER L R POLCAWICH RDRL SER P AMIRTHARAJ
1 (PDF)	UNAFFILIATED ANGELA MAIO

INTENTIONALLY LEFT BLANK.